ChemElectroChem

Research Article
doi.org/10.1002/celc.202300554

Chemistry Europe
European Chemical Societies Publishing

www.chemelectrochem.org

Effects of Anions and Surface Structure on Pt Single Crystal Dissolution in Acidic Electrolytes

Valentín Briega-Martos,*[a] Timo Fuchs,[b] Jakub Drnec,[c] Olaf M. Magnussen,[b] and Serhiy Cherevko*[a]

Understanding the mechanisms of Pt dissolution with well-defined surfaces is vital for developing stable catalysts for electrochemical energy conversion devices such as fuel cells. This work investigates Pt dissolution from low-index single crystals in perchlorate, sulfate, and methanesulfonate acid solutions by on-line inductively coupled plasma mass spectrometry (ICP-MS), and the results are correlated with surface X-ray diffraction (SXRD) studies. The previously reported stability trend Pt(111) > Pt(100) > Pt(110) in $HClO_4$ was confirmed for the other acids. The application of electrochemical protocols up to high potential values demonstrated that dissolution for Pt(100) increases to a lower extent than for the other planes. Dissolution is affected by the nature of the anion, especially for Pt(111), with the dissolution rate increasing in the order H_2SO_4 > MSA > $HClO_4$. This influence could be due to the interaction strength of the anion with Pt and its complexing ability or different ratios of the surface coverage of different oxide species. For Pt(111), SXRD measurements show different onset potentials for extraction in $HClO_4$ and H_2SO_4, which can influence the dissolution processes. These results demonstrate that fundamental studies are necessary to improve the current knowledge about Pt dissolution and how to hinder it to a practical extent.

Introduction

Polymer electrolyte membrane fuel cells (PEMFCs) are regarded as key energy conversion devices for transitioning to a greener and more sustainable energy landscape, because of their high efficiency and energy density, as well as their compatibility with renewable sources and modern energy carriers.[1] However, PEMFCs still are plagued by some drawbacks that hinder them from becoming commercial technology.[2] One of the reasons is the sluggish kinetics of the oxygen reduction reaction (ORR), which takes place on the cathode of a PEMFC. Pt nanoparticles supported on carbon support are usually employed as the cathode material since Pt is the best pure metal for this reaction. Nevertheless, there are still considerable overpotentials associated with the ORR, even for Pt. Due to that, high Pt loadings for the cathode are necessary to catalyze the ORR at acceptable rates, increasing the cost of these systems. In addition, carbon-supported Pt nanoparticles are subject to different degradation mechanisms, such as Pt dissolution and redeposition, carbon corrosion, agglomeration, Ostwald ripening and particle detachment,[3] decreasing the active surface area and, in turn, the electrocatalytic efficiency, leading to higher overpotentials. Since dissolution is a primary degradation mechanism, different approaches have been developed to improve Pt stability, including protecting low-coordinated sites with Au,[4] using a gold underlayer,[5] alloying with low quantities of Au,[6] controlling the surface structure of the Pt nanoparticles,[7] using matrix supports with tunable conductivity,[8] and modifying the electrocatalyst surface with ionic liquids.[9] In any case, the number of works regarding surface engineering towards increased stability of Pt electrocatalysts is still scarce compared to the importance of this topic, indicating that further improvements in this direction are needed. Deeper fundamental knowledge on the oxidation and dissolution mechanisms of unmodified Pt surfaces is required to design new strategies for improving the electrocatalyst's stability. Additionally, it is also necessary to determine the best operating conditions of Pt-based electrocatalysts in terms of stability.

The first studies of Pt dissolution dependence on electrochemical potential were based on evaluating the change of electrochemically active surface area (ECSA) or measuring the amount of dissolved Pt ex-situ by mass spectrometry after accelerated stress tests (ASTs) simulating the operating conditions of practical devices applied to polycrystalline Pt or carbon-supported Pt nanoparticles.[10] From these works, it was deduced that dissolution takes place when Pt is subjected to oxidative potentials, and additional dissolution occurs when the

[a] Dr. V. Briega-Martos, Dr. S. Cherevko
Helmholtz-Institute Erlangen-Nürnberg for Renewable Energy (IEK-11), Forschungszentrum Jülich
Cauerstr. 1, 91058 Erlangen, Germany
E-mail: v.briega@fz-juelich.de
s.cherevko@fz-juelich.de

[b] T. Fuchs, Prof. O. M. Magnussen
Institut für Experimentelle und Angewandte Physik, Christian-Albrechts-Universität zu Kiel
Olshausenstr. 40, 24098 Kiel, Germany

[c] Dr. J. Drnec
Experimental division, European Synchrotron Radiation Facility
71 Avenue des Martyrs, 38000 Grenoble, France

Supporting information for this article is available on the WWW under https://doi.org/10.1002/celc.202300554

surface Pt oxides are reduced. Pt^{2+} and Pt^{4+} species were experimentally observed and suggested as dissolution products.[10b,c] Pt dissolution was also studied in-situ by electrochemical quartz crystal microbalance (EQCM), and it was observed that degradation in the presence of chlorides is more notorious for nanoparticles than for electrodeposited platinum.[11] Another more recent study by EQCM established that the mass increase due to Pt oxidation is higher in alkaline than in acidic media, but the differences in dissolution are smaller.[12]

The fundamental knowledge about Pt dissolution was substantially improved since the apparition of on-line electrochemical inductively coupled plasma mass spectrometry (ICP-MS) techniques. An electrochemical scanning flow cell (SFC)[13] can be connected to an ICP-MS in order to obtain time- and potential-resolved dissolution data from the working electrode.[14] In the first works by Topalov et al. on polycrystalline Pt it was proposed that Pt dissolution is a transient phenomenon that starts at ca. 1.1 V vs. RHE, and takes place during both positive- and negative-going scans, which is traditionally denominated as anodic and cathodic dissolution, respectively.[15] Anodic dissolution was firstly suggested to be directly determined by the number of low-coordinated sites and almost independent of the anodic limit.[15b] Later studies in the potential range below 1.1 V vs. RHE showed increased anodic dissolution when increasing the upper anodic limit and pointed out that other different explanations are possible as the origin of the anodic dissolution, including the formation and dissolution of a transient oxide or the direct electrochemical dissolution of non-passivated metallic Pt atoms.[16] Cathodic dissolution depends on the amount of oxide formed and the timescale, and therefore is strongly dependent on the anodic and cathodic limits. Pt dissolution was compared in acidic and alkaline media and it was observed that the transient dissolution was doubled in alkaline solution.[17] Temperature-dependent studies showed that higher temperatures lead to higher dissolved amounts during the oxidative scan, whereas the cathodic dissolution decreases.[18] Dissolution of Pt nanoparticles supported on carbon (Pt/C) has also been studied in previous works, showing qualitatively the same behavior as a polycrystalline Pt surface.[19] Nevertheless, these systems are challenging to investigate since additional parameters, such as the particle size and morphology or the interparticle distance, play a significant role.[20]

Despite the high number of studies performed with polycrystalline Pt and Pt nanoparticles, their poorly defined structure only allows proposing tentative mechanisms for Pt dissolution, as the precise arrangement within the Pt surface oxides is unknown. The use of well-defined surfaces of Pt single crystal electrodes is mandatory for a deeper understanding of the Pt dissolution mechanisms. Lopes et al. were the first to couple electrochemical measurements with Pt single crystals to the ICP-MS by using a rotating disk electrode (RDE) configuration with a stationary probe through which the dissolved species were transported to the mass spectrometer (SPRDE-ICP-MS).[21] By using this technique it was pointed out that the stability of the Pt low index planes follows the order Pt(110) < Pt(100) < Pt(111). The SPRDE-ICP-MS setup also demonstrated that Pt stability can be increased by using a gold underlayer and gold atoms to protect the Pt low-coordinated sites.[5] Experiments where the SFC-ICP-MS technique was applied to single crystal electrodes confirmed the stability trend for the Pt basal planes, which was mainly attributed to the surface structure energies and atoms coordination, with the most packed surfaces being the most stable.[22]

From the above it is clear that the Pt surface oxidation and re-structuring processes are intimately related to the dissolution behavior. However, a full microscopic picture of the mechanisms of Pt oxidation and dissolution requires data on the atomic-scale surface structure in addition to the electrochemical and ICP-MS results. In this regard, in-situ studies by high-energy surface X-ray diffraction (SXRD) have been extremely useful in obtaining direct experimental evidence of the changes on the Pt surface during the oxidation-reduction processes.[23] The combination of SXRD structural data and SFC-ICP-MS dissolution results together with DFT calculations allowed proposing different oxidation mechanisms for Pt(111) and Pt(100).[24] While for Pt(111) the Pt atoms in the initial oxide lie directly on top of the original sites, for Pt(100) a less stable stripe oxide structure with laterally shifted Pt atoms is formed, as confirmed by the dissolution results. In a more recent study, where we performed a strict comparison between SXRD and dissolution experiments, the model for Pt(100) oxidation and dissolution was expanded, showing that two different Pt oxide structures are formed during Pt oxidation, and that anodic and cathodic dissolution processes are related to each of those species separately.[25]

Regarding dissolution experiments with well-defined surfaces, further measurements with a wider variety of electrochemical protocols, especially with incursions into higher anodic potential values, are still required to obtain more details about the dissolution processes. In addition, the effect of different anions in the acid electrolyte has still not been studied in detail for Pt single-crystals. In our latest work, no significant differences of the Pt oxide structure on Pt(100) in perchloric and sulphuric acid were detected, but the analogous dissolution experiments were performed only for perchloric acid.[25] In the work by Lopes et al. the effect of the presence of little amounts of chlorides in perchloric acid solutions was examined, but they did not investigate the effect of other common anions with weaker interactions with the Pt surface.[21a] Furuya et al. studied the influence of perchloric, sulphuric, and thifluoromethanesulfonic acid (TFMSA) on polycrystalline Pt, and it was reported that for high concentrations the dissolved amounts follow the trend $H_2SO_4 > TFMSA > HClO_4$.[26] However, since concentration, and not pH, was controlled in these measurements, it is not possible to discard that the observed trend is due to pH differences between the solutions, since dissolution decreases when going from acid to more neutral pH values as pointed out by Topalov et al.[15b] A comparison between perchloric and sulphuric acid was performed by EQCM and it was stated that no important differences can be inferred, although the results show a slightly higher dissolution in the case of sulphuric acid.[12] Hence, a detailed study of the effect of the anion species of commonly used acid electrolytes, which may acts as

reference results for a better understanding of the mechanisms of Pt dissolution in different conditions, can be helpful for the scientific community in this field.

This work investigates the dissolution of the three Pt basal planes in perchloric, sulphuric and methanesulfonic acid (MSA) electrolytes with strict control of the pH using three different electrochemical protocols. The three acids were selected based on the different adsorption strengths with the Pt surface. MSA was also selected to mimic the Pt/electrolyte interface in PEMFCs. The electrochemical protocols were carefully chosen to obtain different types of information from the on-line dissolution data. SXRD results in $HClO_4$ and H_2SO_4 are also compared in order to obtain further insights about the oxidation and dissolution processes taking place. The results presented here improve the current knowledge about the effect of surface structure and anion species on Pt dissolution and pave the way for future studies to obtain further details about the exact Pt dissolution mechanisms.

Experimental

Three different acidic working electrolytes were prepared from $HClO_4$ (70%, Merck Suprapur®), H_2SO_4 (96%, Merck Suprapur®), and CH_3SO_3H (methanesulfonic acid for synthesis, Sigma-Aldrich) with strict concentration control for having the same pH value in all cases (pH = 1.2). The pH was checked electrochemically by measuring the open circuit potential (OCP) of a Pt wire cleaned by flame-annealing against a Ag/AgCl (sat. KCl, Metrohm) reference electrode in the H_2-saturated electrolyte of interest. Starting from the equation that converts the potential measured against the Ag/AgCl electrode (*E (vs. Ag/AgCl)*) to the RHE scale (*E (vs. RHE)*) (Equation 1):

$$E\ (vs.\ RHE) = E\ (vs.\ Ag/AgCl) + E^{0'}_{Ag/AgCl} + 0.059 \times pH \quad (1)$$

where $E^{0'}_{Ag/AgCl}$ is the potential of the Ag/AgCl reference electrode, the pH of the solution can be calculated from the OCP measurement using the following equation (taking into account that *OCP (vs. RHE) = 0* in the H_2-saturated solution) (Equation 2):

$$pH = \frac{-OCP\ (vs.\ Ag/AgCl) - E^{0'}_{Ag/AgCl}}{0.059} \quad (2)$$

$E^{0'}_{Ag/AgCl}$ was carefully determined before the experiments according to the following method. In the first place, a pH = 7 KH_2PO_4/K_2HPO_4 buffer solution was prepared, and its exact pH was measured with a properly calibrated pHmeter (Mettler Toledo, FiveEasy Plus).The exactitude of this pH value (*pH (buffer)*) is highly reliable since the pH of the buffer mixture is in the center of the calibration curve of the pH meter. Secondly, the OCP of a clean Pt wire immersed in the H_2-saturated KH_2PO_4/K_2HPO_4 solution was measured against the Ag/AgCl reference electrode (*OCP (buffer vs. Ag/AgCl)*) for calculating $E^{0'}_{Ag/}$AgCl (Equation 3):

$$E^{0'}_{Ag/AgCl} = -OCP\ (buffer, vs.\ Ag/AgCl) - 0.059 \times pH\ (buffer) \quad (3)$$

Before each electrochemical measurement, the working Pt(111), Pt(100) and Pt(110) (99.999%, Mateck) single crystal electrode disks were flame-annealed in a propane-flame, cooled down in a Ar/H_2 (3:1) reducing mixture and protected with an ultrapure water drop satured with these gases to avoid the oxidation and contamination of the surface during its transfer to the electrochemical cell. The cooling atmosphere mentioned above generates experimental surface structures that agree with the nominal topographies.[27] Pt(110) surfaces can change from a (1×1) unreconstructed surface to a (1×2) missing-row surface.[28] Since the cyclic voltammetry profiles obtained here in H_2SO_4 are very similar to the ones for the (1×1) surface in ref. [28a], but not identical to the one presented in ref. [28b] after CO cooling in $HClO_4$, we can conclude that the surfaces obtained in this work are mixed (1×1)/(1×2) surfaces with major (1×1) contributions.[29]

Reference cyclic voltammetries for all the surface orientations and electrolytes were recorded in a classical glass bulk electrochemical cell. A flame-annealed Pt wire quenched with ultrapure water and a Ag/AgCl reference electrode in a second compartment separated by a Luggin capillary were used as counter and reference electrode, respectively. The working solution was deoxygenated with Ar (99.999%, Air Liquide). All the glassware was thoroughly cleaned by the traditional permanganate method,[30] which started by soaking the material overnight in a ca. 2 g L^{-1} $KMnO_4$ and dilute H_2SO_4 mixture. Once the $KMnO_4$ solution was recovered, the glassware was rinsed with a 1% H_2O_2 and 0.1 M H_2SO_4 solution to remove the traces of manganese species. Finally, the glassware was boiled in ultrapure water (18.2 MΩ cm, Merck Milli-Q IQ 7000) at least four times to eliminate the remaining traces of organic and anion species that could specifically adsorb on the Pt surface.

The electrochemical on-line SFC-ICP-MS measurements were performed using a glassy carbon rod (HTW Sigradur G) counter electrode and a Ag/AgCl (sat. KCl, Metrohm) reference electrode. The reference electrode is placed after the outlet of the SFC to avoid chlorides contamination. The SFC-ICP-MS system requires special conditions of cleanliness and the absence of oxygen in the working electrolyte when working with Pt single crystals to ensure that other undesired effects do not influence the surface structure dependence. Firstly, most parts of the setup were substituted by glass-made variants (electrolyte reservoir, purge vial, some tubings), which can be intensively cleaned, for example, by the previously explained permanganate method. The glass parts also avoid the entrance of oxygen into the system to a better extent. Secondly, the SFC, usually custom-made from polycarbonate, was substituted by a PTFE version to allow analogous cleaning for the glass parts of the setup. In addition, the SFC was fabricated with a shield around the electrolyte outlet through which the working solution is contacted to prevent oxygen in the meniscus with the electrode surface (Figure 1a). Finally, a new holder for the Pt single crystals was developed, allowing a larger area surrounding the electrode disk and favoring an optimum argon flow around the electrolyte meniscus (Figure 1b). These improvements in the SFC-ICP-MS systems permitted obtaining cyclic voltammetry results for the three Pt basal planes almost identical to those obtained in a classic glass bulk cell (Figure 1c), demonstrating the system's suitability for getting reliable surface structure-dependent results.[31]

The working electrolyte was constantly provided to the purge vial of the SFC through a peristaltic pump (Ismatec), where the working electrolyte was purged with Ar. The solution circulated through the SFC to the ICP-MS (NexION™ 350X, PerkinElmer) by equilibrating the Ar flow in the purge vial and the speed of the peristaltic pump (MP2, Elemental Scientific) of the ICP-MS. A ca. 200 μL min^{-1} flow rate, precisely determined for each measurement, was employed. The dissolution of ^{195}Pt from the working electrode was tracked with the ICP-MS via previous calibration with Pt standard solutions (0, 0.5, 1 and 5 μg L^{-1}, Certipur, Merck). ^{187}Re was the internal standard using a 10 μg L^{-1} Re solution (Certipur, Merck). The working area of the electrode in contact with the solution was 0.159 cm^2. Total dissolved amounts in mML were calculated by integrating the peaks in the measured dissolution profiles and

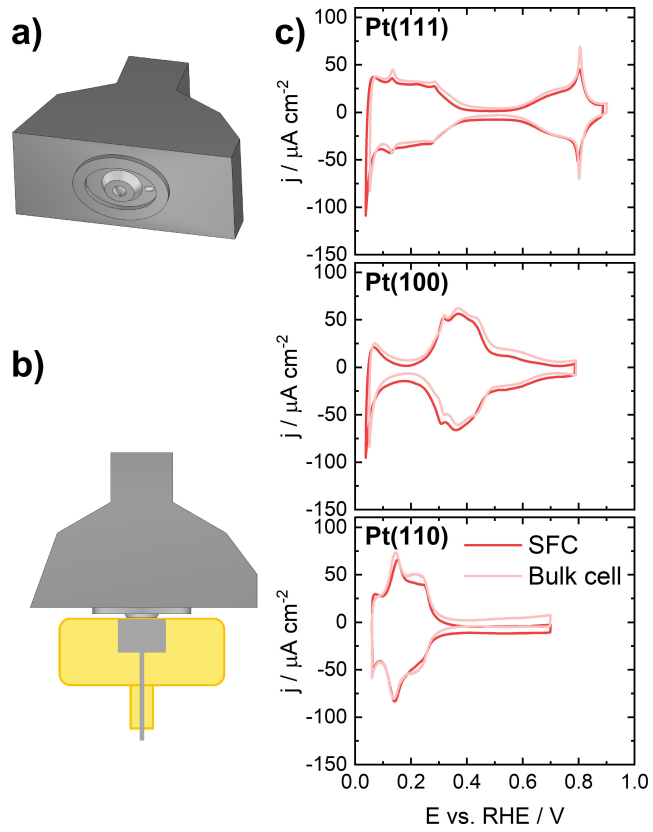

Figure 1. a) Detailed view of the shield on the PTFE SFC used in this work. b) Sketch of SFC (top grey part) and the Pt single crystal holder (bottom yellow piece surrounding the grey single crystal disk) to ensure and optimum argon flow and absence of oxygen during the SFC-ICP-MS measurements. c) Cyclic voltammetry profiles for the three basal planes in $HClO_4$ (pH = 1.2) obtained in the SFC system (red) and a glass bulk cell (pale red).

converting from ng cm^{-2} by using the surface atomic density for each orientation ($1.49 \cdot 10^{15}$, $1.30 \cdot 10^{15}$ and $9.19 \cdot 10^{14}$ atoms cm^{-2} for Pt(111), Pt(100) and Pt(110), respectively). Please note that, although the studied Pt(110) surfaces are probably a mixture of (1×1) and (1×2) contributions as stated above, the surface atomic density for an ideal unreconstructed Pt(110) is considered since we the exact role of the different surface sites (i.e. sites on reconstructed and unreconstructed Pt) is unknown. In any case, assuming that the behavior of both types of sites is the same, since we already took the most packed as possible Pt(110) surface, if we would consider a less packed surface the differences in dissolved amounts in mML between Pt(110) and the other two basal planes would be even higher than the ones shown here.

The different electrochemical protocols were applied using a Gamry Reference [600] potentiostat. The working electrode was always contacted to the electrolyte at a controlled potential of 0.1 V vs. RHE in order to avoid any possible surface oxidation before the measurement.

Three protocols were involved in this work:

- *Protocol 1* consisted of consecutive cyclic voltammetries at a scan rate of 10 mV s^{-1} with 0.05 V vs. RHE as lower potential limit (LPL) and 0.8 to 1.9 V vs. RHE as upper potential limit (UPL), increasing the latter in 0.1 V after each cylic voltammetry.
- *Protocol 2*, two cyclic voltammetries at 2 mV s^{-1} were performed with 0.05 V vs. RHE as LPL and 1.2 and 1.6 V vs. RHE as UPL for the first and second cycle, respectively.
- *Protocol 3* comprises a potential jump from 0.05 V vs. RHE to 1.6 V vs RHE, followed by a potential hold at 1.6 V vs. RHE during 300 seconds, and finalized with a potential sweep at 10 mV s^{-1} from 0.05 V to 1.6 V vs. RHE.

All potentials in this work were converted to the RHE scale using equation (1), and measurements were performed at room temperature (21 °C).

Surface X-ray diffraction studies were performed employing a hanging meniscus electrochemical cell with an upward facing crystal surface, which is described in detail in previous studies.[24–25] The counter electrode was a Pt foil. The reference electrode was a leak-free Ag/AgCl electrode (eDaq) attached to an additional glass capillary with a Pt wire junction, which served as Luggin capillary. All glassware and electrolyte carrying cell components were cleaned following the procedure described above. Tubes and syringes were thoroughly rinsed with the ultrapure water.

The high energy surface X-ray diffraction measurements were carried out at beamline ID31 of the European Synchrotron ESRF with a photon energy of 78 keV and a beam size of 12×48 µm^2 (vertical×horizontal). The stationary X-ray detector (Dectris Pilatus 2 M CdTe) with an active surface area of 253.7×288.8 mm^2 was placed 71 cm behind the Pt single crystal electrode. Its precise position was determined by the analysis of the Debye-Scherrer rings of a CeO_2 powder diffraction standard (NIST) using the pyFAI software.[32] With this detector positioning it was possible to collect scattering angles which correspond to a momentum transfer in the range of ±7 Å^{-1} horizontally and up to 15 Å^{-1} vertically. To protect the X-ray detector from radiation damage, the positions where intense Bragg reflections can hit the detector during the measurement were covered by about 80 cylindrical Tungsten beamstop pieces with a diameter of 5–10 mm about 1 cm in front of the detector. To reduce the air background scattering, an additional Tungsten beamstop with a diameter of 3 mm was placed about 10 cm behind the Pt single crystal at the primary beam position. The photocurrent of a photodiode pointed at a thin Aluminium foil, which was placed in the incident beam, was used to correct the measured intensities for the small fluctuations of the incident photon flux. For further details about the acquisition of the CTRs and their analysis and fitting procedures the reader is referred to our previous works.[24–25]

Results

Before the on-line dissolution and SXRD experiments, the three Pt basal planes in contact with the different electrolyte solutions under study were characterized in an electrochemical glass bulk cell. The left panels in Figure 2 show the cyclic voltammetry profiles when the UPLs are restricted to values below which there is no oxidation and restructuring of the surface. The obtained results in $HClO_4$ and H_2SO_4 agree with the previous literature, demonstrating the good quality of the Pt single crystals and the electrolytes employed.[31] The case of Pt(111) in $HClO_4$ displays two well-separated regions. The region below 0.40 V vs. RHE, which remains unaffected by the nature of the anions in the solution, corresponds to the hydrogen adsorption/desorption region. In contrast, the anion adsorption is displaced to potentials higher than 0.55 V vs. RHE for $HClO_4$, while for H_2SO_4 it starts right after the hydrogen desorption signal. It is generally accepted that perchlorate anions interact

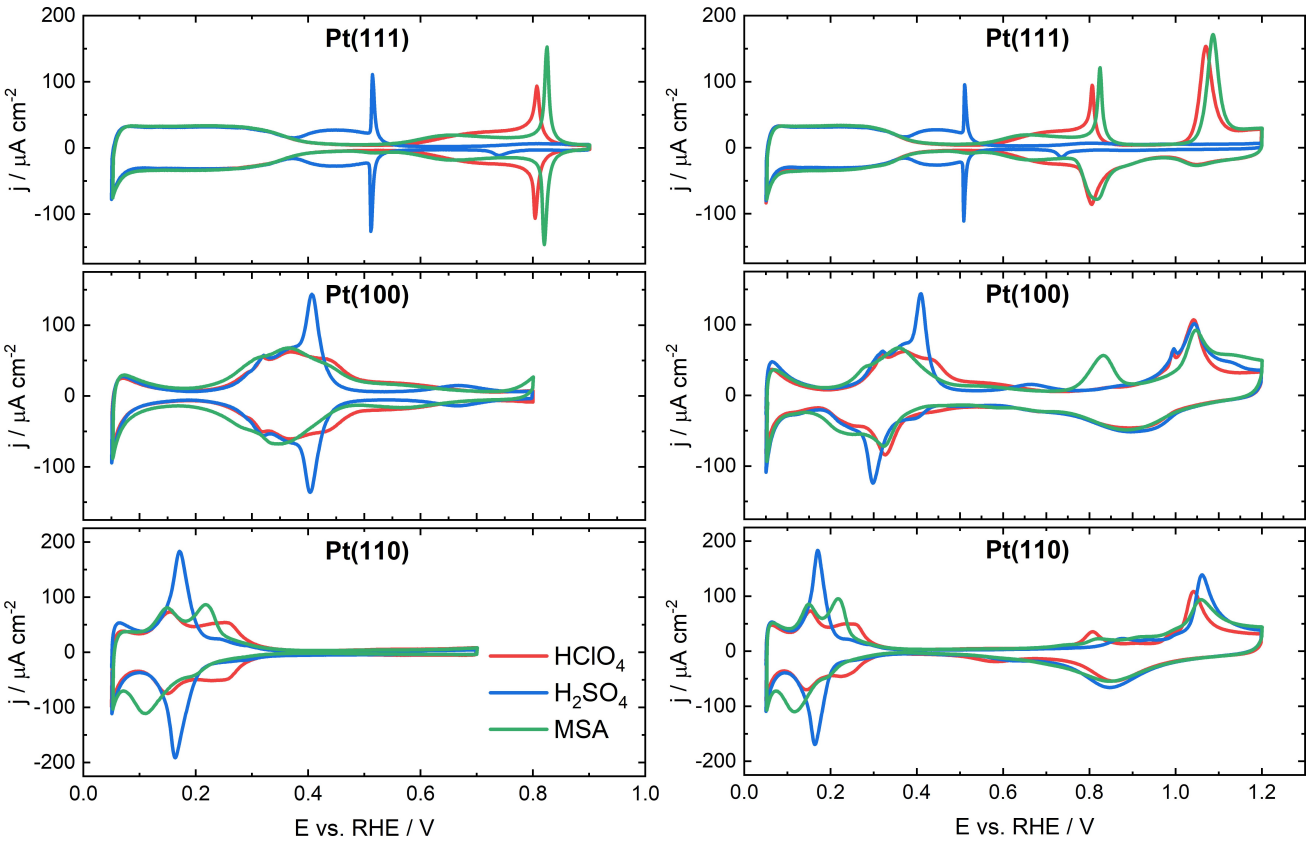

Figure 2. Cyclic voltammetry profiles for the three Pt basal planes in $HClO_4$ (red), H_2SO_4 (blue) and MSA (green) electrolytes with pH = 1.2. The UPLs are adjusted for each basal plane in order to avoid surface disorder in the left panels, while the UPL is 1.2 V vs. RHE for all orientations in the right panels. Scan rate: 50 mV s^{-1}.

very weakly with the Pt surface and therefore it does not adsorb specifically, while sulfate anions adsorb strongly on Pt. In the case of H_2SO_4 it was demonstrated by CO charge displacement experiments that sulfates start adsorbing on Pt(111) from 0.30 V vs. RHE,[33] and the sharp spike at ca. 0.5 V vs. RHE arises from the disordered-ordered phase transition of the sulfate adlayer. For $HClO_4$, the similarity of the cyclic voltammetry profile in comparison with other weakly adsorbing anions like fluoride[29,34] allowed to discard the hypothesis that the signal above 0.55 V is due to perchlorate adsorption. Consequently, this feature can be ascribed to the adsorption of OH species.[35] For Pt(100) and Pt(110), hydrogen desorption and anion adsorption are coupled. Sulfate adsorption compresses the adsorption states in a narrower potential region, while in solutions containing non-specifically adsorbing anions the signals are broader.[36]

The case of MSA has not been studied extensively in the past. Sandoval et al. investigated the electrochemical interface of the Pt low-index planes in 0.1 M MSA, showing identical results to the ones presented in Figure 2.[37] The absence of MSA bands in in-situ infrared spectroscopy experiments and the similarity of the cyclic voltammetry profiles to the ones in $HClO_4$ led the authors to propose that MSA does not adsorb specifically on Pt. However, they suggested that the slight differences between $HClO_4$ and MSA are because methanesulfonate anion is a potent kosmotrope agent, an interfacial structure maker.[35] In any case, the authors did not discard the adsorption of small amounts of methanesulfonate on the surface that would be below the detection limit of the infrared spectroscopy measurements, especially for the Pt(100) surface. In conclusion, MSA can be considered to have an intermediate interaction strength with Pt between $HClO_4$ and H_2SO_4. It is also important to mention that methanesulfonic acid is more prone to have small amounts of impurities and/or products of decomposition, which may be responsible for the observed asymmetries in the cyclic voltammetry profiles for Pt(100) and Pt(110).

The right panels in Figure 2 show the cyclic voltammetry results for the three Pt basal planes when surface oxidation up to 1.2 V vs. RHE occurs. The anodic peak centered at 1.07 V vs. RHE for Pt(111) in $HClO_4$ is traditionally assigned to the further oxidation of PtOH to PtO, and with the help of SXRD measurements, it was observed that this process is coupled to a reversible place exchange in which a Pt atom exchanges with an oxygen species.[23a,38] It can be observed that the presence of methanesulfonate anions slightly shifts this signal to more positive potential values, while in H_2SO_4 solution it is totally suppressed up to 1.2 V vs. RHE. Figure 3 shows the X-ray intensity in $HClO_4$ and H_2SO_4 recorded simultaneously during a cyclic voltammogram at 20 mV s^{-1}. As seen in Figure 3 and indicated in the Supporting Table S1, from these data it can be deduced that the onset potential for Pt place exchange in the

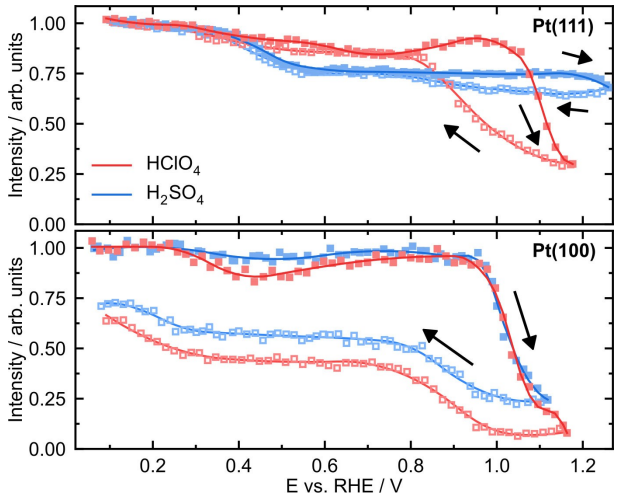

Figure 3. Relative changes in X-ray intensity near anti-Bragg positions of the crystal truncation rods for (a) Pt(111) and (b) Pt(100) in $HClO_4$ (red) and H_2SO_4 (blue) during cyclic voltammograms at 20 mV s^{-1}. The onset of Pt place exchange manifest in form of a decrease in intensity at potentials positive of 0.95 V.

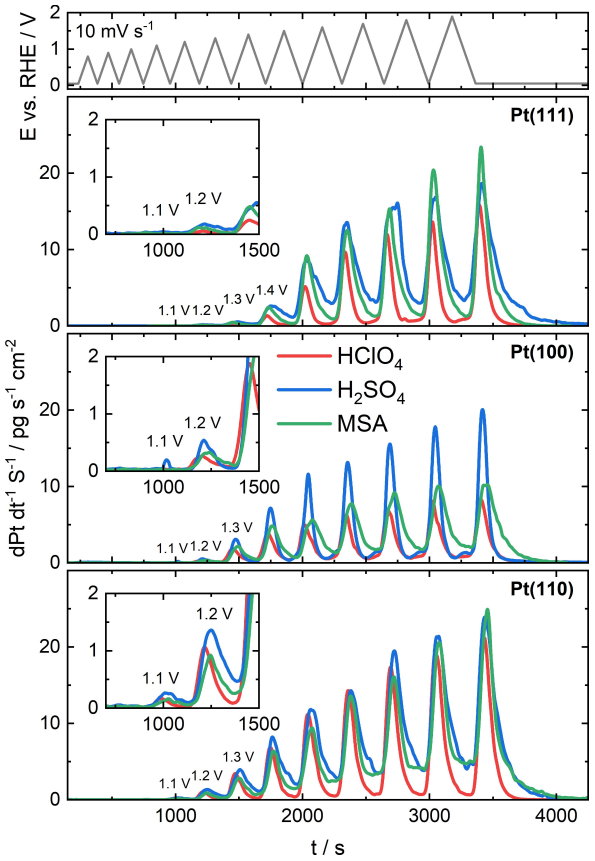

Figure 4. Electrochemical program used for *Protocol 1* (top panel). Dissolution profiles for Pt(111), Pt(100) and Pt(110) corresponding to *Protocol 1* in $HClO_4$ (red), H_2SO_4 (blue) and MSA (green) with pH = 1.2.

case of the Pt(111) is 1.05 V for $HClO_4$, while it is 1.17 V for H_2SO_4. The different behaviour of the X-ray intensity in the region of the butterfly peak can be assigned to the formation of the well-known ordered sulfate adlayer, which affects the diffraction rod. The higher onset potential for oxidation in H_2SO_4 correlates well with the cyclic voltammogram at high potentials suggesting that no place-exchange takes place until ca. 1.2 V vs. RHE in the case H_2SO_4. In contrast, for the case of Pt(100), the structure and potential-dependence of the formed oxide phases is very similar in $HClO_4$ and H_2SO_4 solution, as depicted in Figure 3 and Table S1, which is in agreement with the similar voltammetric response in the Pt oxidation regime.[24–25] Here, the onset of oxidation in the positive going potential sweep is almost identical in the two electrolytes. The offset between the X-ray intensity curves in the reverse sweep is a consequence of the 50 mV more positive UPL in $HClO_4$ solution and the strong irreversibility of the Pt extraction process on the Pt(100) surface. The situation is more complex for Pt(110) and ongoing investigations are trying to clarify the origin of the oxidation and the associated oxide species formed on this surface.

The initial electrochemical protocol used for the on-line dissolution measurements consisted of applying successive potential cycles at 10 mV s^{-1}, in which the UPL was increased by 0.1 V after each cycle (*Protocol 1*). This protocol was used for obtaining information about the onset potential of Pt dissolution on the different surface orientations and in different electrolytes. It also allows comparing the dissolved amounts and how they evolve with consecutive cycling. The applied electrochemical protocol and the corresponding dissolution profiles are presented in Figure 4.

The first aspect that can be pointed out is that for an UPL of 1.1 V vs. RHE no dissolution is observed for Pt(111) in any of the studied electrolytes, minimal signals are measured for Pt(100), and noticeable dissolution peaks appear for Pt(110). This is in agreement with the previous studies in 0.1 M $HClO_4$, which proposed as stability order Pt(111) > Pt(100) > Pt(110).[21a,22] It is important to remark that in the case of Pt and the conditions of the employed electrochemical protocols, cathodic dissolution is the main contribution to the dissolution signal. In the successive cycles to increasingly higher UPLs, the dissolved amounts per cycle increase less for Pt(100) than for the other two basal planes. The effect of the nature of the anion species in the different acidic solutions is studied in detail here for the first time. From the dissolution profiles, it can be seen that dissolution is in general lower for the $HClO_4$ solution. The dissolution peaks in Figure 4 were integrated to obtain the absolute dissolved quantities in ng cm^{-2} in order to get more quantitative information regarding the dissolved amounts in the different acid electrolytes. The ng cm^{-2} amounts were converted to mML by considering each orientation's distinct surface atomic density, and the results are displayed in Figure 5. The anion effects are the strongest in the case of Pt(111), with dissolved amounts following the order H_2SO_4 > MSA > $HClO_4$. The differences are not so apparent for the other basal planes, but $HClO_4$ shows the lowest dissolution in all cases.

The second electrochemical protocol for the SFC-ICP-MS measurements consisted of two consecutive slow cycles at 2 mV s^{-1} with 1.2 and 1.6 V vs. RHE as UPL (*Protocol 2*), and the results are shown in Figure 6 (Figure S1 displays the same

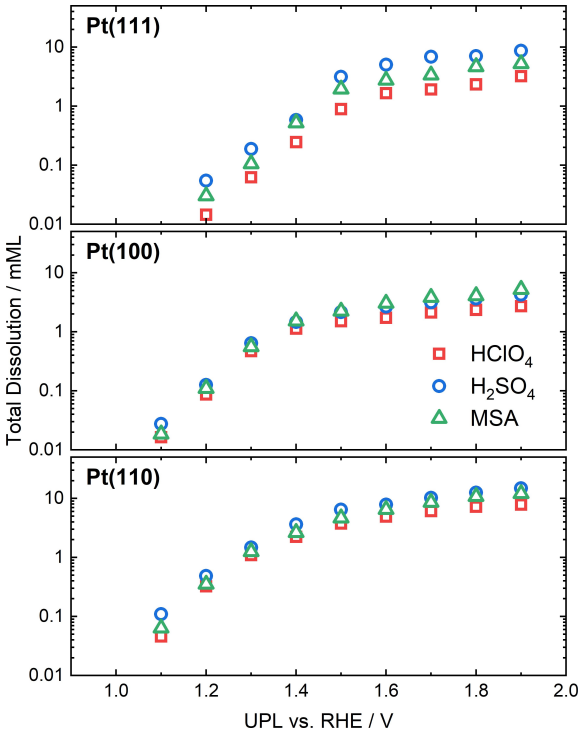

Figure 5. Dissolved amounts (in logarithmic scale) for each consecutive cycle at different UPLs during *Protocol 1* in Figure 4.

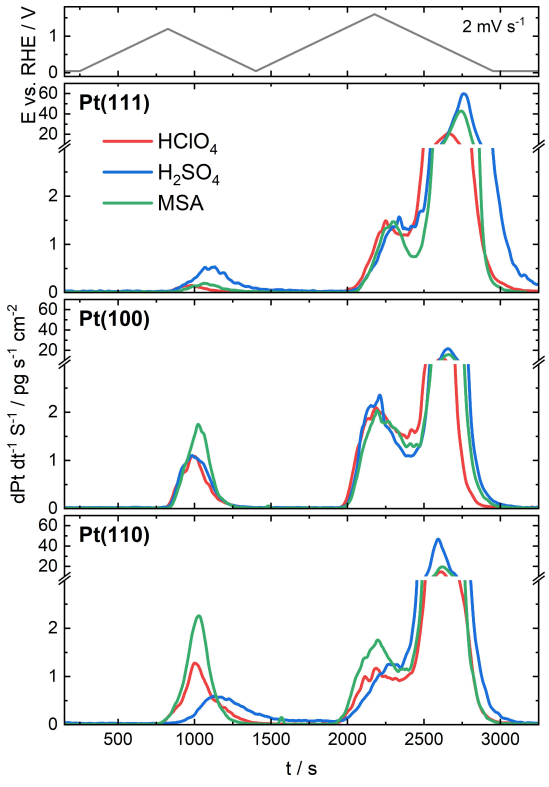

Figure 6. Electrochemical program used for *Protocol 2* (top panel). Dissolution profiles for Pt(111), Pt(100) and Pt(110) corresponding to *Protocol 2* in $HClO_4$ (red), H_2SO_4 (blue) and MSA (green) with pH = 1.2.

measurements without the break in the y-axis). Compared to *Protocol 1*, this protocol allows for inspecting the onset potentials of dissolution more accurately and resolving the anodic and cathodic dissolution contributions in the case of the cyclic voltammetry up to 1.6 V vs. RHE.[15] The dissolved amounts for the CV up to 1.2 V vs. RHE agree with the stability order previously observed, Pt(111) > Pt(100) > Pt(110). However, the differences are not so clear for the anodic scan up to 1.6 V vs. RHE, and for the cathodic scan the dissolution for Pt(100) is the lowest. The anion effect for Pt(111) in the cycle with an UPL of 1.2 V vs. RHE is the same as pointed out by *Protocol 1*, but no significant differences in the anodic dissolution are visible in the cycle to the high UPL. The anion effects are more notable in the case of the cathodic dissolution, for which the dissolution order $H_2SO_4 > MSA > HClO_4$ is observed for the three orientations. Furthermore, the width of the dissolution peak depends on the anion species, especially for Pt(110), where the dissolution peak is noticeable broader in sulfuric acid than in the other electrolytes, suggesting slower dissolution kinetics.

Onset potentials of dissolution were extracted from the semilogarithmic representation of Figure 6 (the reader is referred to Figure S2 for an example) and presented in Figure 7. The presented anodic dissolution onset potentials correspond to the first cyclic voltammogram with UPL 1.2 V vs. RHE for Pt(100) and Pt(110) and to the second cyclic voltammogram with UPL 1.6 V vs. RHE for Pt(111). The onset potentials of cathodic dissolution were determined in an analogous way from the rise of the dissolution signal during the negative-going scan of the second cyclic voltammetry up to 1.6 V vs. RHE. The anodic dissolution onset potentials are the lowest for $HClO_4$ for all the Pt basal planes, while the highest values correspond to H_2SO_4. On Pt(111), this could be explained by the 0.13 V vs. RHE more positive onset of place-exchange in H_2SO_4, shown in Figure 3. In the case of cathodic dissolution, the earliest onset potential from the start of the negative-going ramp (the most positive onset potential) takes place for $HClO_4$, except for

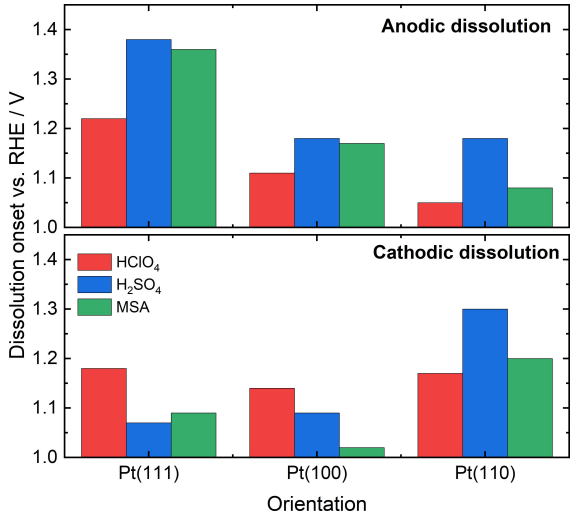

Figure 7. Onsets for anodic dissolution (top) and cathodic dissolution (bottom) extracted from *Protocol 2* for Pt(111), Pt(100) and Pt(110) in $HClO_4$ (red), H_2SO_4 (blue) and MSA (green) with pH = 1.2.

Pt(110), for which it corresponds to H_2SO_4. However, the determination of this value can be influenced by the fact that the anodic dissolution signal is broader for H_2SO_4 in the case of Pt(110).

Finally, an electrochemical protocol with a potential hold at an oxidative potential of 1.6 V vs. RHE followed by a reductive ramp was investigated (*Protocol 3*). Analogous protocols were employed in the past to analyze the possible effect of re-deposition in the dissolution signal and for direct comparison with SXRD measurements.[25,39] This protocol allows to study the influence of long residence times at a constant oxidative potential. Furthermore, it is also helpful to completely separate the anodic and cathodic dissolution signal. The left panels in Figure 8 shows the dissolution profiles corresponding to this protocol while the right panel displays the current density responses. No clear trends can be deduced from the dissolution signal during the oxidative peak, most likely because 1.6 V vs. RHE is very disruptive for the well-defined surfaces and also surface passivation by the oxides plays a role. Anodic dissolution is significantly higher for Pt(110), in accordance with the generally observed trend. Regarding the cathodic dissolution during the reductive ramp, the lowest signals correspond to Pt(100), which agrees with the results of the other two protocols at high potentials. The highest dissolution values are reached in H_2SO_4 solution for all the orientations, but for this protocol the trend is not that pronounced for Pt(111) as in the previous cases. This is probably because the hold at high oxidative potentials during 5 minutes already significantly disordered the surface. In the right panels of Figure 8, the corresponding current reduction peaks are presented to allow correlation of the measured dissolved amounts with the reductive charge, which is related to the amount of surface oxides formed.[15b,25] It can be observed that the charge follows the order $H_2SO_4 < MSA < HClO_4$, while cathodic dissolution follows in general the opposite trend. Therefore, there is not a directly proportional relationship between reductive charge and dissolved amount. Figure 8 also show that different values for the reductive charge are obtained when comparing the three orientations. Further discussions regarding this will be presented in the next section.

Discussion

The cyclic voltammetry profiles presented in Figure 2 reflect the different degrees of interaction of the employed anions with

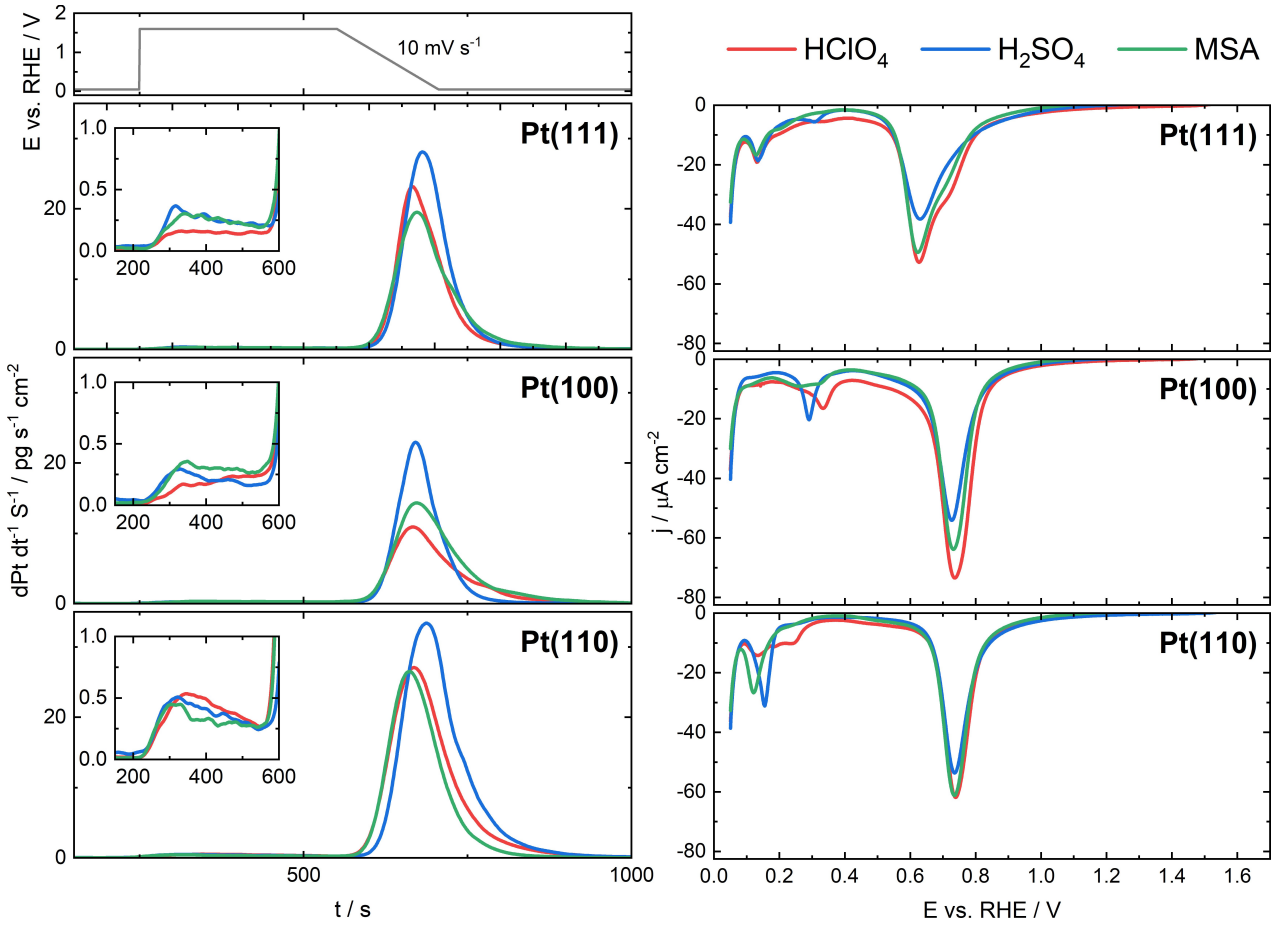

Figure 8. Left: Electrochemical program used for *Protocol 3* (top panel). Dissolution profiles for Pt(111), Pt(100) and Pt(110) corresponding to *Protocol 3* in $HClO_4$ (red), H_2SO_4 (blue) and MSA (green) with pH = 1.2. Right: Current density response corresponding to the potential ramp of *Protocol 3* depicted in the left panels.

the Pt surface. Consequently, the lower stability against dissolution generally observed for H_2SO_4, especially in the case of Pt(111), may indicate that a strong adsorption of the anion on Pt could promote dissolution. Jerkiewicz et al. also observed more dissolution for polycrystalline Pt in 0.5 M H_2SO_4 solution after an AST protocol compared to $HClO_4$.[26] However, they performed an experiment adding 10^{-2} M H_2SO_4 to the 0.5 M $HClO_4$ solution and did not observe appreciable differences in dissolution when compared with the sulfate-free electrolyte. Therefore, they concluded that anion adsorption has negligible impact on Pt dissolution, and they proposed that the higher dissolution in the case of 0.5 M H_2SO_4 is due to the different equilibrium constants of the Pt^{2+}- and Pt^{4+}-containing complex compounds.[26] Differences in dissolution in their case could also be due to changes in pH, since the parameter they controlled was the anion concentration.

One may also attempt to correlate the oxidation peaks in the cyclic voltammograms with the corresponding dissolution profiles. According to Figure 2 the onset for PtO formation on Pt(111) is slightly displaced to more positive values for MSA with respect to $HClO_4$, while for H_2SO_4 the Pt oxidation is fully inhibited for potentials up to 1.2 V. This is in line with the trend of the onset potential for dissolution displayed in Figure 7 for Pt(111). The inhibited Pt oxidation in H_2SO_4 correlates well with the SXRD data shown in Figure 3 for Pt(111), indicating that the place-exchange does not take place until ca. 1.2 V vs. RHE, most likely due to sulphate adsorption. The place-exchange is fully reversible in $HClO_4$, and this is in agreement with the absence of dissolution at potentials lower than 1.2 V vs. RHE in this case.[24] In contrast, the place exchange on Pt(111) in H_2SO_4 is immediately irreversible, which again correlates well with the dissolution data. Similar correlations between dissolution and the onset of oxidation, as determined from the electrochemical response, could be established for Pt(110). For Pt(100), the anodic dissolution behaviour is very similar in H_2SO_4 and $HClO_4$, which is in line with the very similar onset of oxidation according to the SXRD and electrochemical data. Whether the same is true for Pt(100) in MSA is unclear at present due to the lack of SXRD results in this electrolyte. Conversely, it is not possible to establish clear correlations of the dissolution with the onset of the reduction peaks, since the current density responses are very similar for the different electrolytes. This could be due to the existence of different surface oxides with varying dissolution behaviours, as we already demonstrated for Pt(100) in $HClO_4$ solution, and different chemical dissolution mechanisms, as pointed out by Jerkiewicz et al.[26] and more recently by Cho et al.[40]

In the case of *Protocol 3*, anodic dissolution during the oxidative hold is clearly lower in the case of $HClO_4$ for both Pt(111) and Pt(100). On the basis of combined SFC-ICP-MS and in-situ SXRD results for Pt(100) it was proposed that anodic dissolution for this type of protocol is directly related to an initially formed oxide species, consisting of oxide stripes that are commensurate to the underlying metal lattice.[25] Comparison of the X-ray intensity for an oxidation and reduction cycle in 0.1 M $HClO_4$ and 0.1 M H_2SO_4 allowed to conclude that the nature of the anion has no major influence on the Pt(100) oxide structure and its initial formation kinetics.[25] This experiment used a comparable potential program as the SFC-ICP-MS experiments employing protocol 2, where the anodic dissolution behaviour of Pt(100) was found to be almost independent of the anion species, in excellent agreement with the SXRD results.

The opposite trend between cathodic dissolution during *Protocol 3* and the corresponding reductive charges during the ramp is remarkable. The corresponding charges have been integrated from the reduction peak in the current-potential response in Figure 8 and have been plotted in Figure 9 for clarity. Topalov et al. observed a positive linear relationship between the cathodic charge and dissolved amounts when comparing cyclic voltammetry experiments performed at different scan rate and using Pt-poly electrodes,[15b] suggesting that cathodic dissolution is directly proportional to the reduction charge, that is, to the amount of previously formed oxide. However, according to the results presented in this work a higher amount of formed oxide not always leads to higher cathodic dissolution for different surface structures or working electrolytes. It is important to remark that in studies as the above-mentioned comparison when using different scan rates, the other experimental conditions stay the same (surface structure, anions nature, pH, temperature…), and therefore the formed surface oxide structure and other processes as complexing reactions and redeposition rates are comparable between measurements, allowing making the direct correlation between charge and dissolved amounts. On the contrary, in the present work we use surfaces with different orientation and electrolytes with different anions. In the case of Pt(100), we showed by SXRD that for high oxidative potentials a second oxide structure is formed, which corresponds to a more disordered oxide phase where the Pt atoms are located further away from the surface. The comparison with on-line dissolution measurements suggested that cathodic dissolution is directly related with this second oxide species.[25] A similar behaviour with two different oxide species may be expected for the other two Pt basal

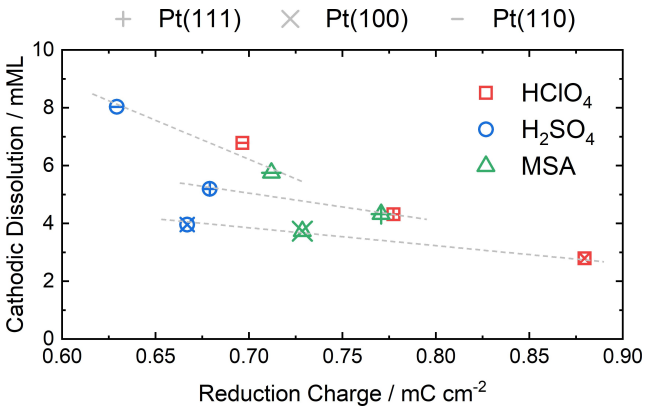

Figure 9. Cathodic dissolution amounts obtained from the integration of the corresponding dissolution peaks vs. the corresponding reduction charge plot from *Protocol* 3 for Pt(111) (plus sign), Pt(100) (multiplication sign) and Pt(110) (minus sign) in $HClO_4$ (red), H_2SO_4 (blue) and MSA (green). Grey dashed lines are added to help differentiate between the data of the different basal planes.

planes, although it has not been clearly demonstrated yet.[23d,24–25] The results presented here could be explained by a scenario where the fraction of the different oxide species depend on the surface orientation and the anion present in the electrolyte. In this scenario, the higher reduction charge but lower cathodic dissolution in the case of Pt(100) would be correlated with a lower fraction of the disordered oxide phase in the total surface oxide. Similarly, the higher cathodic dissolution but lower reduction charge in the experiments in sulphuric acid would suggest a higher fraction of the more disordered oxide, which could be influenced by the different interaction strength of the anions. As already mentioned, a possible different complexing by the different anion species cannot be discarded[26,40] and also different redeposition mechanisms and kinetics could play a role.[39] However, for Pt(111) and Pt(100) the highest reduction charge and lowest dissolution occur for $HClO_4$ while in the case of Pt(110) these occur for MSA. This seem to indicate that there must be a structure influence apart from a purely chemical effect due the nature of the anion. The results highlight the need of more combined SXRD and on-line dissolution studies supported by calculation, e.g. density functional theory (DFT)[24–25,41] and molecular dynamic (MD)[42] simulations for the different Pt well-defined surfaces and various possible electrolytes, which we plan to carry out in future studies.

Conclusions

The effect of surface structure and anion species in acid electrolytes on the dissolution of the three Pt basal planes was investigated using three custom designed protocols in $HClO_4$, H_2SO_4, and MSA electrolytes with precise pH control (1.2). The SFC-ICP-MS was previously optimized in order to meet the strict working standards for Pt single crystals electrochemistry. Cyclic voltammograms of these systems are in agreement with the previous literature and indicate that $HClO_4$ possesses the weakest interaction with Pt, MSA does not adsorb specifically or to a low extent and affects the interfacial water structure, and H_2SO_4 exhibits strong specific adsorption on the Pt surface, especially on Pt(111). In on-line dissolution experiments where the potential does not exceed 1.2 V vs. RHE, Pt(111) and Pt(110) are the most stable and least stable surfaces, respectively, as reported in the previous studies in $HClO_4$. Our results also confirm this trend for dissolution in MSA and H_2SO_4. However, stability does not vary to the same extent for the three basal planes when excursions to higher potentials are performed and dissolution for Pt(100) is the lowest at high potentials. Regarding the influence of the anion species present in the acid electrolytes, there is a clear dependence for Pt(111), where the lowest dissolution is found for $HClO_4$ and the highest for H_2SO_4. This can be correlated with the differences in the onset potential for extraction measured in $HClO_4$ and H_2SO_4 by SXRD. This trend in the stability also is observed for the cathodic dissolution during cyclic voltammetry up to 1.6 V vs. RHE. Nevertheless, for experiments employing a reductive ramp after an oxidative hold at high potential, the comparison of the current density and the dissolution profile the total amount of formed surface oxides was not clearly correlated with the amount of dissolved Pt. This was also found when comparing different surface orientations and could be due to differences in the surface fraction of coexisting oxide species and in the complexing strength of the present anions. These observations show that a consistent microscopic picture of Pt oxidative dissolution is still missing. Further on-line dissolution studies coupled with new HESXRD measurement experiments and DFT and MD calculations are necessary to clarify the origin of the differences in stability found for different anion species and to obtain deeper insights into the re-structuring processes in the different media.

Supporting Information

SXRD Data about the onset potentials for extraction for Pt(111) and Pt(100) in $HClO_4$ and H_2SO_4, the dissolution profiles for *Protocol 2* without break in the y-axis, and the determination method of the onset potential of dissolution can be found in the Supporting Information.

Acknowledgements

The SXRD experiments were performed on beamline ID31 at the European Synchrotron Radiation Facility (ESRF), Grenoble, France. Funding is acknowledged from Deutsche Forschungsgemeinschaft for OMM and SC (project number 418603497). Open Access funding enabled and organized by Projekt DEAL.

Conflict of Interests

The authors declare no conflict of interest.

Data Availability Statement

The data that support the findings of this study are available from the corresponding author upon reasonable request.

Keywords: dissolution · electrochemistry · mass spectrometry · platinum · single crystals

[1] a) B. G. Pollet, S. S. Kocha, I. Staffell, *Curr. Opin. Electrochem.* **2019**, *16*, 90–95; b) R. Borup, J. Meyers, B. Pivovar, Y. S. Kim, R. Mukundan, N. Garland, D. Myers, M. Wilson, F. Garzon, D. Wood, P. Zelenay, K. More, K. Stroh, T. Zawodzinski, J. Boncella, J. E. McGrath, M. Inaba, K. Miyatake, M. Hori, K. Ota, Z. Ogumi, S. Miyata, A. Nishikata, Z. Siroma, Y. Uchimoto, K. Yasuda, K. I. Kimijima, N. Iwashita, *Chem. Rev.* **2007**, *107*, 3904–3951; c) C. S. Gittleman, A. Kongkanand, D. Masten, W. B. Gu, *Curr. Opin. Electrochem.* **2019**, *18*, 81–89.
[2] M. K. Debe, *Nature* **2012**, *486*, 43–51.
[3] a) T. Zhang, P. Q. Wang, H. C. Chen, P. C. Pei, *Appl. Energy* **2018**, *223*, 249–262; b) J. C. Meier, C. Galeano, I. Katsounaros, J. Witte, H. J. Bongard, A. A. Topalov, C. Baldizzone, S. Mezzavilla, F. Schuth, K. J. J. Mayrhofer, *Beilstein J. Nanotechnol.* **2014**, *5*, 44–67.

[4] J. Zhang, K. Sasaki, E. Sutter, R. R. Adzic, *Science* **2007**, *315*, 220–222.
[5] P. P. Lopes, D. G. Li, H. F. Lv, C. Wang, D. Tripkovic, Y. S. Zhu, R. Schimmenti, H. Daimon, Y. J. Kang, J. Snyder, N. Becknell, K. L. More, D. Strmcnik, N. M. Markovic, M. Mavrikakis, V. R. Stamenkovic, *Nat. Mater.* **2020**, *19*, 1207–1214.
[6] X. Xie, V. Briega-Martos, R. Farris, M. Dopita, M. Vorokhta, T. Skala, I. Matolinova, K. M. Neyman, S. Cherevko, I. Khalakhan, *ACS Appl. Mater. Interfaces* **2023**, *15*, 1192–1200.
[7] V. Mastronardi, E. Magliocca, J. S. Gullon, R. Brescia, P. P. Pompa, T. S. Miller, M. Moglianetti, *ACS Appl. Mater. Interfaces* **2022**, *14*, 36570–36581.
[8] M. Smiljanic, M. Bele, L. J. Moriau, J. F. V. Santa, S. Menart, M. Sala, A. Hrnjic, P. Jovanovic, F. Ruiz-Zepeda, M. Gaberscek, N. Hodnik, *ACS Omega* **2022**, *7*, 3540–3548.
[9] G. R. Zhang, T. Wolker, D. J. S. Sandbeck, M. Munoz, K. J. J. Mayrhofer, S. Cherevko, B. J. M. Etzold, *ACS Catal.* **2018**, *8*, 8244–8254.
[10] a) C. A. Reiser, L. Bregoli, T. W. Patterson, J. S. Yi, J. D. L. Yang, M. L. Perry, T. D. Jarvi, *Electrochem. Solid-State Lett.* **2005**, *8*, A273–A276; b) L. Y. Xing, G. Jerkiewicz, D. Beauchemin, *Anal. Chim. Acta.* **2013**, *785*, 16–21; c) L. Y. Xing, M. Hossain, M. Tian, D. Beauchemin, K. Adjemian, G. Jerkiewicz, *Electrocatalysis* **2014**, *5*, 96–112; d) Z. Q. Wang, E. Tada, A. Nishikata, *J. Electrochem. Soc.* **2014**, *161*, F380–F385.
[11] A. B. Ofstad, M. S. Thomassen, J. L. G. de la Fuente, F. Seland, S. Moller-Holst, S. Sunde, *J. Electrochem. Soc.* **2010**, *157*, B621–B627.
[12] L. Strandberg, V. Shokhen, M. Luneau, G. Lindbergh, C. Lagergren, B. Wickman, *ChemElectroChem* **2022**, *9*, e20220059.
[13] A. K. Schuppert, A. A. Topalov, I. Katsounaros, S. O. Klemm, K. J. J. Mayrhofer, *J. Electrochem. Soc.* **2012**, *159*, F670–F675.
[14] a) O. Kasian, S. Geiger, K. J. J. Mayrhofer, S. Cherevko, *Chem. Rec.* **2019**, *19*, 2130–2142; b) S. Cherevko, K. J. J. Mayrhofer, in *Encyclopedia of Interfacial Chemistry. Surface Science and Electrochemistry* (Ed.: K. Wandelt), Elsevier, Oxford **2018**, pp. 326–355.
[15] a) A. A. Topalov, I. Katsounaros, M. Auinger, S. Cherevko, J. C. Meier, S. O. Klemm, K. J. J. Mayrhofer, *Angew. Chem. Int. Ed.* **2012**, *51*, 12613–12615; b) A. A. Topalov, S. Cherevko, A. R. Zeradjanin, J. C. Meier, I. Katsounaros, K. J. Mayrhofer, *Chem. Sci.* **2014**, *5*, 631–638.
[16] S. Cherevko, G. P. Keeley, S. Geiger, A. R. Zeradjanin, N. Hodnik, N. Kulyk, K. J. J. Mayrhofer, *ChemElectroChem* **2015**, *2*, 1471–1478.
[17] S. Cherevko, A. R. Zeradjanin, G. P. Keeley, K. J. J. Mayrhofer, *J. Electrochem. Soc.* **2014**, *161*, H822–H830.
[18] S. Cherevko, A. A. Topalov, A. R. Zeradjanin, G. P. Keeley, K. J. Mayrhofer, *Electrocatalysis* **2014**, *5*, 235–240.
[19] a) A. Pavlisic, P. Jovanovic, V. S. Selih, M. Sala, N. Hodnik, M. Gaberscek, *J. Electrochem. Soc.* **2018**, *165*, F3161–F3165; b) P. Jovanovic, U. Petek, N. Hodnik, F. Ruiz-Zepeda, M. Gatalo, M. Sala, V. S. Selih, T. P. Fellinger, M. Gaberscek, *Phys. Chem. Chem. Phys.* **2017**, *19*, 21446–21452.
[20] a) D. J. S. Sandbeck, M. Inaba, J. Quinson, J. Bucher, A. Zana, M. Arenz, S. Cherevko, *ACS Appl. Mater. Interfaces* **2020**, *12*, 25718–25727; b) D. J. S. Sandbeck, N. M. Secher, F. D. Speck, J. E. Sorensen, J. Kibsgaard, I. Chorkendorff, S. Cherevko, *ACS Catal.* **2020**, *10*, 6281–6290; c) D. J. S. Sandbeck, N. M. Secher, M. Inaba, J. Quinson, J. E. Sorensen, J. Kibsgaard, A. Zana, F. Bizzotto, F. D. Speck, M. T. Y. Paul, A. Dworzak, C. Dosche, M. Oezaslan, I. Chorkendorff, M. Arenz, S. Cherevko, *J. Electrochem. Soc.* **2020**, *167*; d) H. Schmies, A. Bergmann, E. Hornberger, J. Drnec, G. X. Wang, F. Dionigi, S. Kuhl, D. J. S. Sandbeck, K. J. J. Mayrhofer, V. Ramani, S. Cherevko, P. Strasser, *Phys. Chem. Chem. Phys.* **2020**, *22*, 22260–22270.
[21] a) P. P. Lopes, D. Strmcnik, D. Tripkovic, J. G. Connell, V. Stamenkovic, N. M. Markovic, *ACS Catal.* **2016**, *6*, 2536–2544; b) P. P. Lopes, D. Tripkovic, P. F. B. D. Martins, D. Strmcnik, E. A. Ticianelli, V. R. Stamenkovic, N. M. Markovic, *J. Electroanal. Chem.* **2018**, *819*, 123–129.
[22] D. J. S. Sandbeck, O. Brummel, K. J. J. Mayrhofer, J. Libuda, I. Katsounaros, S. Cherevko, *ChemPhysChem* **2019**, *20*, 2997–3003.
[23] a) J. Drnec, M. Ruge, F. Reikowski, B. Rahn, F. Carla, R. Felici, J. Stettner, O. M. Magnussen, D. A. Harrington, *Electrochim. Acta* **2017**, *224*, 220–227; b) M. Ruge, J. Drnec, B. Rahn, F. Reikowski, D. A. Harrington, F. Carla, R. Felici, J. Stettner, O. M. Magnussen, *J. Electrochem. Soc.* **2017**, *164*, H608–H614; c) J. Drnec, D. A. Harrington, O. M. Magnussen, *Curr. Opin. Electrochem.* **2017**, *4*, 69–75; d) L. Jacobse, V. Vonk, I. T. McCrum, C. Seitz, M. T. M. Koper, M. J. Rost, A. Stierle, *Electrochim. Acta* **2022**, *407*, 139881; e) T. Fuchs, V. Briega-Martos, J. O. Fehrs, C. R. Qiu, M. Mirolo, C. T. Yuan, S. Cherevko, J. Drnec, O. M. Magnussen, D. A. Harrington, *J. Phys. Chem. Lett.* **2023**, 3589–3593.
[24] T. Fuchs, J. Drnec, F. Calle-Vallejo, N. Stubb, D. J. S. Sandbeck, M. Ruge, S. Cherevko, D. A. Harrington, O. M. Magnussen, *Nat. Catal.* **2020**, *3*, 754–761.
[25] T. Fuchs, V. Briega-Martos, J. Drnec, N. Stubb, I. Martens, F. Calle-Vallejo, D. A. Harrington, S. Cherevko, O. M. Magnussen, *Angew. Chem. Int. Ed.* **2023**, *62*, e202304293.
[26] Y. Furuya, T. Mashio, A. Ohma, M. Tian, F. Kaveh, D. Beauchemin, G. Jerkiewicz, *ACS Catal.* **2015**, *5*, 2605–2614.
[27] E. Herrero, J. M. Orts, A. Aldaz, J. M. Feliu, *Surf. Sci.* **1999**, *440*, 259–270.
[28] a) N. M. Markovic, B. N. Grgur, C. A. Lucas, P. N. Ross, *Surf. Sci.* **1997**, *384*, L805-L814; b) G. A. Attard, A. Brew, *J. Electroanal. Chem.* **2015**, *747*, 123–129.
[29] V. Briega-Martos, E. Herrero, J. M. Feliu, *Electrochim. Acta* **2017**, *241*, 497–509.
[30] a) C. Korzeniewski, V. Climent, J. M. Feliu, in *Electroanalytical Chemistry: A Series of Advances, Vol. 24* (Eds.: A. J. Bard, C. Zoski), CRC Press, Taylor & Francis Group, Boca Raton **2012**, pp. 75–169; b) N. Arulmozhi, D. Esau, J. van Drunen, G. Jerkiewicz, *Electrocatalysis* **2018**, *9*, 113–123.
[31] V. Climent, J. M. Feliu, in *Advances in Electrochemical Science and Engineering: Nanopatterned and Nanoparticle-Modified Electrodes, Vol. 17* (Eds.: R. C. Alkire, P. N. Bartlett, J. Lipkowski), Wiley-VCH Verlag GmbH & Co. KGaA Weinheim **2017**, pp. 1–57.
[32] J. Kieffer, V. Valls, N. Blanc, C. Hennig, *J. Synchrotron Radiat.* **2020**, *27*, 558–566.
[33] J. M. Feliu, J. M. Orts, R. Gomez, A. Aldaz, J. Clavilier, *J. Electroanal. Chem.* **1994**, *372*, 265–268.
[34] a) F. C. Nart, T. Iwasita, M. Weber, *Electrochim. Acta* **1994**, *39*, 961–968; b) V. Briega-Martos, W. Cheuquepan, J. M. Feliu, *J. Phys. Chem. Lett.* **2021**, *12*, 1588–1592.
[35] A. Berna, V. Climent, J. M. Feliu, *Electrochem. Commun.* **2007**, *9*, 2789–2794.
[36] J. Clavilier, J. M. Orts, R. Gómez, J. M. Feliu, A. Aldaz, in *The Electrochemical Society Proceedings, Vol. 94–21* (Eds.: B. E. Conway, G. Jerkiewicz), The Electrochemical Society, Inc., Pennington, NJ **1994**, pp. 167–183.
[37] A. P. Sandoval, M. F. Suaez-Herrera, V. Climent, J. M. Feliu, *Electrochem. Commun.* **2015**, *50*, 47–50.
[38] a) A. M. Gomez-Marin, J. Clavilier, J. M. Feliu, *J. Electroanal. Chem.* **2013**, *688*, 360–370; b) H. You, D. J. Zurawski, Z. Nagy, R. M. Yonco, *J. Chem. Phys.* **1994**, *100*, 4699–4702.
[39] C. Stumm, S. Grau, F. D. Speck, F. Hilpert, V. Briega-Martos, K. Mayrhofer, S. Cherevko, O. Brummel, J. Libuda, *J. Phys. Chem. C* **2021**, *125*, 22698–22704.
[40] J. S. Cho, H. Kim, H. S. Oh, C. H. Choi, *JACS Au* **2023**, *3*, 105–112.
[41] a) Y. F. Huang, P. J. Kooyman, M. T. M. Koper, *Nat. Commun.* **2016**, *7*; b) X. T. Chen, I. T. McCrum, K. A. Schwarz, M. J. Janik, M. T. M. Koper, *Angew. Chem. Int. Ed.* **2017**, *56*, 15025–15029.
[42] a) J. B. Le, A. Chen, L. Li, J. F. Xiong, J. G. Lan, Y. P. Liu, M. Iannuzzi, J. Cheng, *JACS Au* **2021**, *1*, 569–577; b) A. Gross, S. Sakong, *Curr. Opin. Electrochem.* **2019**, *14*, 1–6; c) H. H. Kristoffersen, T. Vegge, H. A. Hansen, *Chem. Sci.* **2018**, *9*; d) O. M. Magnussen, A. Gross, *J. Am. Chem. Soc.* **2019**, *141*, 4777–4790.

Manuscript received: October 13, 2023
Revised manuscript received: November 29, 2023
Version of record online: January 16, 2024